



## Verification of Application of ANN Modelling in Study of Compressive Behaviour of Aluminium Sponges

Anna M. STREK<sup>1</sup>\*, Marek DUDZIK<sup>2</sup>), Arkadiusz KWIECIEŃ<sup>1</sup>)  
Krzysztof WAŃCZYK<sup>3</sup>), Barbara LIPOWSKA<sup>4</sup>)

<sup>1</sup>) *Cracow University of Technology*  
*Faculty of Civil Engineering*  
*Institute of Structural Mechanics*

Warszawska 24, 31-155 Kraków, Poland

\*Corresponding Author e-mail: anna.strek@pk.edu.pl

<sup>2</sup>) *Cracow University of Technology*  
*Faculty of Electrical and Computer Engineering*  
*Department of Traction and Traffic Control*

Warszawska 24, 31-155 Kraków, Poland

<sup>3</sup>) *Foundry Research Institute*  
*Center for Design and Prototyping*  
Zakopiańska 73, 30-418 Kraków, Poland

<sup>4</sup>) *Institute of Ceramics and Building Materials*  
*Refractory Materials Division in Gliwice*  
Toszecka 99, 44-100 Gliwice, Poland

This article presents a preliminary neural network analysis of the compressive behaviour of aluminium open-cell sponges and answers the question of whether this phenomenon can be modelled using artificial intelligence. The research consisted of two phases: first – compression experiments, which in turn provided data for the second phase – the artificial neural network (ANN) analysis. A two-argument function was proposed and tested using the gathered experimental data with a two-layer feedforward network. The determination coefficient  $R^2$  for linear correlation between targets and modelling outputs was chosen as the criterion for the assessment of the quality of modelling. The obtained values were  $R^2 > 0.96$ , which shows that neural networks hold the capacity to address the characterisation of the mechanical response of aluminium open-cell sponges in compression. Additionally, the mean absolute relative error (MARE) and the mean square error (MSE) were also determined.

**Key words:** metal sponges; aluminium sponges; compression tests; artificial neural networks.

## 1. INTRODUCTION

Porous metals are one of the most interesting classes of materials; they find applications in a broad range of fields, such as: medicine, transportation, energy industry etc. [1, 2]. Depending on the type of porosity and skeleton's structure, they are classified to different subgroups: closed-cell metallic materials, open-cell metals, sponges, gasars, and others [3]. Also, various skeleton's materials are used: from aluminium, copper, titanium to even gold and, of course, a scope of alloys [4–10]. This material class is becoming more and more popular.

On the other hand, mechanical description of porous metals is also developing and apart from well-grounded experimental and modelling techniques, like X-ray tomography (e.g. [11, 12]), scanning electron microscopy SEM (e.g. [13, 14]), FEM models (e.g. [15]) and many other classical solutions, new approaches are being introduced (e.g. [16]). One of them is the authors' concept to use artificial neural networks for the modelling of compressive behaviour of open-cell aluminium. ANNs have been already applied with success in mechanical engineering and mechanics of materials [17–19]. The new approach has the following potential advantages: neural network analysis enables one to extend the range of mechanical description beyond actual experimental data and gives the possibility to avoid the need of certain data which might be expensive, time-consuming or difficult to obtain. In other words, ANNs have the capability of overcoming some degree of data lack. This feature of neural networks is used in building metamodels or surrogate models, and also in metallurgy and material engineering (e.g. [20]). However, there are also aspects of the use of neural networks requiring special attention. For example, the network's architecture could be inappropriately structured and as a result could obscure or distance the actual material description.

The presented study is continuation and development of previous work [21, 22]. Compressive behaviour data from experiments carried on 12 samples of aluminium sponge were now to be computationally modelled with the use of ANNs: two two-layer feedforward neural networks, differing in number of neurons in hidden layers, were to be implemented in Matlab and the results were to be compared.

## 2. THE MATERIAL AND UNIAXIAL COMPRESSION TESTS

### *2.1. Samples*

The material was not bought from an external supplier but was self-produced [23] using the lost form casting method [24, 25]. It was an open-cell aluminium sponge with PPI 5.4–6.2, depending on the anisotropy axis. Parameters of the

production method were calibrated in the course of the manufacturing, so there were two sample groups obtained: the prototype group (with some minor structural imperfections and generally larger apparent densities) and the regular group (without visible structural mistakes, with smaller apparent densities). The structural imperfections in the first group of samples included: form residuals sank inside samples, metal drops cast inside, irregular cell shapes. For the purpose of the research, the prototype group was denoted as ‘P’ and the regular group – with the letter ‘R’. Exemplary samples of both types are shown in Fig. 1. Dimensions of the used samples and average apparent densities are shown in Table 1. Samples’ dimensions were chosen such that they satisfy the condition of the minimal number of cells to avoid the scale effect [26].

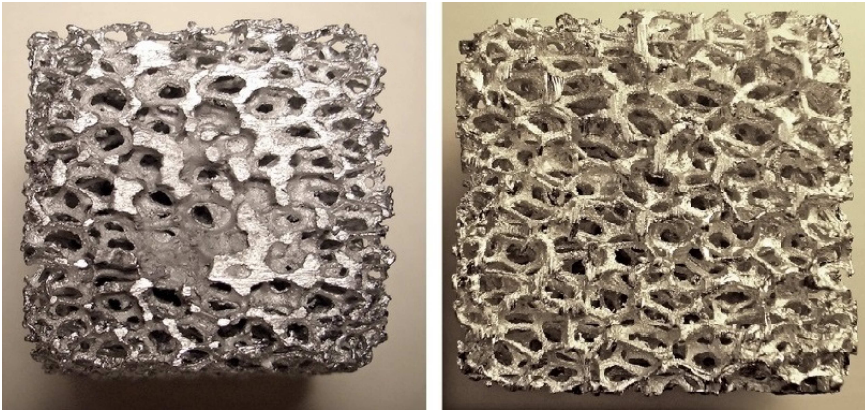


FIG. 1. Samples of the open-cell aluminium; left: type ‘P’ and right: type ‘R’.

**Table 1.** Basic specifications of the produced open-cell aluminium samples.

Parameter	Value
av. PPI	due to anisotropy: 5.4-6.2
av. sample size, ‘P’	53.0 × 39.5 × 39.0 mm
av. sample size, ‘R’	62.8 × 39.5 × 38.0 mm
av. apparent density, ‘P’	0.485 ± 0.010 g/cm <sup>3</sup>
av. apparent density, ‘R’	0.312 ± 0.006 g/cm <sup>3</sup>

## 2.2. Experimental procedure

The tests in the presented research were performed with the use of the Zwick 1455 20 kN machine and the computer programme TestExpert II. The assumed experimental conditions were: initial force 5 N, data acquisition frequency 100 Hz and strain rate 0.5% ·  $L_0$  in mm/s, where  $L_0$  was the initial sample height. Experiments and processing of results were partially conveyed according to [27].

### 2.3. Results of the compression experiments

The graph of stress-strain response of the samples in compression is shown in Fig. 2. Solid lines are for samples of the type ‘P’, while dashed lines are for the ‘R’ group. Along with the stress-strain curves there are depicted values of apparent density in  $\text{g/cm}^3$  for each sample. Different values of samples’ apparent densities were attributed to the influence of structure imperfections in the ‘P’ group, as well as to the stochastic distribution of cell dimensions in the material itself in both groups (compare: [28]).

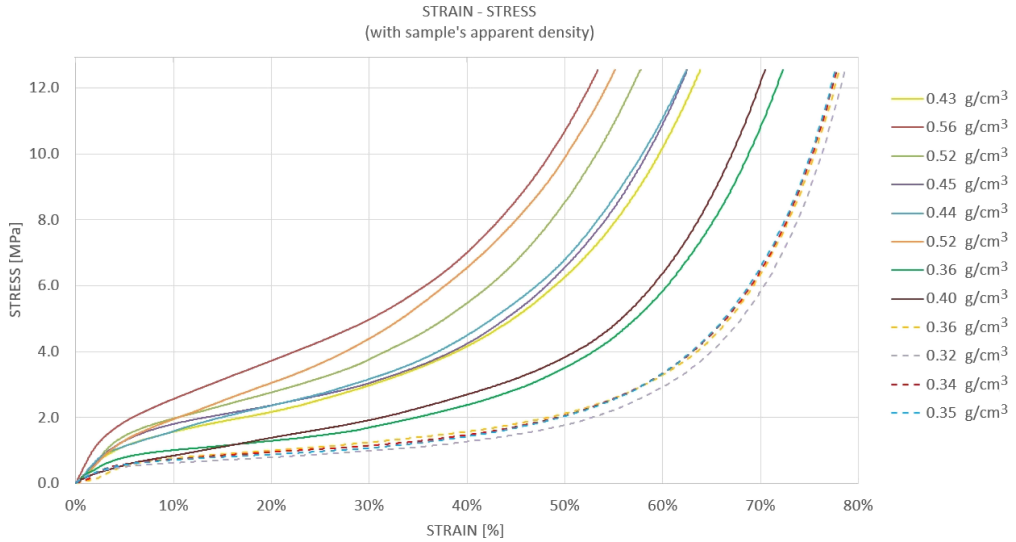


FIG. 2. Stress-strain plots from the compression tests; the numbers by plots are apparent densities in  $\text{g/cm}^3$ . Solid lines represent the prototype group, the dashed lines are for regular samples.

It can be noted that the compressive behaviour is related to the apparent density. Observation of this correlation became the basis for choosing the form of the relation assumed for modelling with ANNs.

## 3. THE ANN ANALYSIS

### 3.1. Formulation of the ANN multiargument approximation

The proposed model of the function relating stress-strain behaviour and apparent density has the following general form:

$$(3.1) \quad \sigma = f(\epsilon, \rho),$$

where  $\sigma$  is stress,  $\epsilon$  is strain and  $\rho$  is apparent density. Such a presumption is justified by well-established theory [29], as well as by experimental curves in Fig. 2. The experimental data from the above described compression tests were used as a matter for the network's learning and its consequent self-testing. Modelling was done in Matlab R2018B using the multi-argument function fitting ANN tool [30–32].

The assessment of the quality of the fitting capability of used network structures was based on the analysis of the relation between targets and corresponding networks outputs. The authors assumed one primary criterion and two auxiliary criteria. The main criterion was the coefficient of determination  $R^2$  for the linear correlation between outputs of the ANN modelling and targets from experiments, and the presumed threshold value was set as 0.9. Additionally, two other measures were introduced as quality indicators: the mean square error (MSE) and the mean absolute relative error (MARE). All measures are explained in Subsec. 3.3.

### 3.2. Data, the ANN's structure and learning parameters

**Data.** All data were taken from the conveyed uniaxial tests. For each sample 1000 experimental strain and respective stress values were taken. These data and appropriate samples' apparent densities were then grouped into sets  $\{\epsilon_i, \rho_i, \sigma_i\}$ , where  $i = 1, 2, \dots, n$ , with  $n = 12 \cdot 1000 = 12000$ . Arguments for ANN were assumed as  $n$  vectors  $\mathbf{Input}_i = [\epsilon_i, \rho_i]^T$ ; the corresponding experimental stresses from  $i$ -th data sets were assumed as the respective  $n$  targets  $\text{Target}_i = \sigma_i$ .

The procedure of normalisation, i.e., the linear transformation of data into the range  $\langle -1, 1 \rangle$ , was performed. Normalisation is not necessary for neural network calculations; however, it is claimed to have good influence on the method's convergence [33]. The Matlab inbuilt function 'mapminmax' was used for this purpose [34–36]. The transformation was done according to Eq. (3.2):

$$(3.2) \quad V' = \frac{V - V_{\min}}{V_{\max} - V_{\min}} \cdot (V'_{\max} - V'_{\min}) + V'_{\min},$$

where  $V$  is the original value,  $V'$  is the transformed value,  $V'_{\max}$  and  $V'_{\min}$  are original range boundaries, and  $V'_{\max}$  and  $V'_{\min}$  are desired range boundaries, here:  $-1$  and  $1$ .

**The ANN's structure.** Before analysis, a general shape of the network had to be chosen as a presumption. Experimental curves showed high non-linearity, yet were smooth and generally similar in shape. This fact constituted the provision that one hidden layer and one output layer should be enough. The non-linearity could be addressed by a non-linear activation function in the hidden layer and then linearised in the output layer. Hence, the authors decided to perform the analysis using a two-layer feedforward neural network implemented in

Matlab. The first layer was the hidden layer, and the second was the output layer. The activation function for the hidden layer was *tansig*, i.e., a hyperbolic tangent sigmoid transfer function, mathematically equivalent to *th* [34]. The output layer had a linear activation function. The chosen architecture is in agreement with the standard solution for fitting problems, which is: “the multilayer perceptron, with *tansig* neurons in the hidden layers and linear neurons in the output layer” [37].

Two variants of the hidden layer were assumed, leading to the creation of two networks. In the first case, the hidden layer consisted of 3 neurons, while in the second one – of 15 neurons (see Fig. 3). The number of neurons was chosen such that they represent a reasonably simple (3) and a complex (15) case [37]. The number of neurons in the output layer was chosen as one in accordance with a single variable output [37].

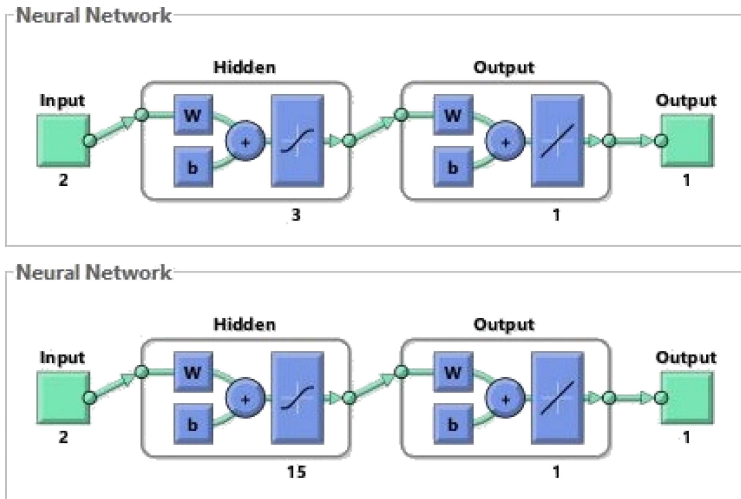


FIG. 3. The used ANN structures. Top: the structure with 3 neurons in the hidden layer; bottom: the structure with 15 neurons in the hidden layer.

**Learning parameters.** The ANN modelling procedure consisted of three stages: training, validation and test. The measurement data was divided in the following proportions between the three steps: 60% for training, 20% for validation and 20% for test. The assumed training algorithm was Levenberg-Marquardt [38–40]<sup>1)</sup> with mean square error (MSE) taken as the performance function. Other training parameters included:

- performance function goal: 0;
- minimum performance gradient:  $10^{-10}$ ;

<sup>1)</sup>According to [41], the algorithm was first reported by LEVENBERG [38] but also independently rediscovered by: MARQUARDT [39], GIRARD [42], WYNNE [43] and MORRISON [44].

- maximum validation failures: 6;
- learning rate: 0.01;
- momentum: 0.9;
- maximum number of epochs to train: 1000.

### 3.3. Results

A summary of numerical values of results is presented in Table 2 and detailed plots are depicted in figures: Fig. 4 – the relation between targets and outputs for the ANN with 3 neurons, Fig. 5 – the relation between targets and outputs for the ANN with 15 neurons, Fig. 6 – error histograms, Fig. 7 – relative error histograms. Figure 8 – the performance function. In the following sections, bottom indices 3n and 15n will be used to indicate whether a discussed magnitude refers to the network with 3 neurons or with 15 neurons, respectively. The terms: correlation coefficient  $R$ , coefficient of determination  $R^2$ , error Err, mean absolute relative error MARE and mean square error MSE will be explained in the course of this section.

**Table 2.** Results from the ANN analysis for the networks with 3 and 15 neurons.

Parameter	3 neurons	15 neurons
correlation coefficient, $R$	0.98265	0.99001
coefficient of determination, $R^2$	0.96560	0.98011
interval of most error instances, $\text{Err}^{\text{most}}$ [MPa]	[-0.7768; 0.5316]	[-0.1477; 0.104 ]
mean absolute relative error, MARE	0.27545	0.09251
mean square error, MSE [MPa <sup>2</sup> ]	0.3107	0.1796
epoch no. for the best validation performance	130	89
epoch no. for validation fail	136	95

**The relation between targets and outputs.** Figures 4 and 5 show outputs  $\sigma_{i,\text{otpt}}$  plotted against targets  $\sigma_i$  for networks with 3 and 15 neurons, respectively. In each figure, both top graphs and bottom left graph depict the correlation between outputs and targets for each learning stage separately: training, validation and test. The bottom right graphs present the correlation between outputs and targets in all learning stages together. The ideal match between approximated and experimentally measured values of stress would result in the following formula:  $\sigma_{\text{otpt}} = 1 \cdot \sigma + 0$ . Formulas for the linear fit obtained for both analysed networks for all learning stages together are close to the ideal approximation formula:

$$\begin{aligned} \sigma_{\text{otpt}.3\text{n}} &= 0.96 \cdot \sigma_{3\text{n}} + 0.13, \\ \sigma_{\text{otpt}.15\text{n}} &= 0.98 \cdot \sigma_{15\text{n}} + 0.06. \end{aligned}$$

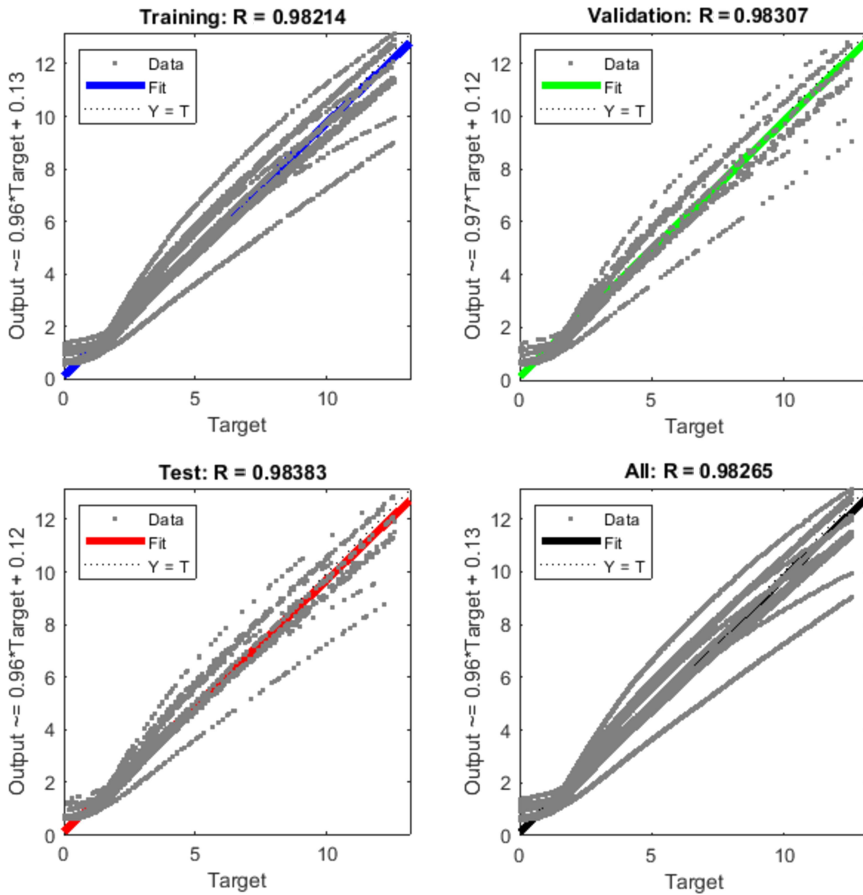


FIG. 4. Linear regression of outputs versus targets for the ANN with 3 neurons in the hidden layer: top left for the training stage, top right for the validation stage, bottom left for the test stage and bottom right for all data.

Two standard indicators of linear correlation were calculated:  $R$  – the Pearson correlation coefficient, and the coefficient of determination  $R^2$ , assumed as the square of the correlation coefficient. Both measures were determined for all three stages (training, validation and test) together. Values of the correlation coefficient were:  $R_{3n} = 0.98265$  and  $R_{15n} = 0.99001$ . The coefficients of determination were equal to:  $R_{3n}^2 = 0.96560$  and  $R_{15n}^2 = 0.98011$ , which means that in both cases the variation of outputs was very well explained with the variation of targets ( $R^2 \geq 0.9 = 90\%$ ).

However, even though numerical values of the  $R^2$  coefficients were in both cases similar and both very good, it can be observed that, when comparing the plots in Figs 4 and 5, the graphs for the ANN with 15 neurons are much closer to a straight line than for the one with 3 neurons. It is a provision that the

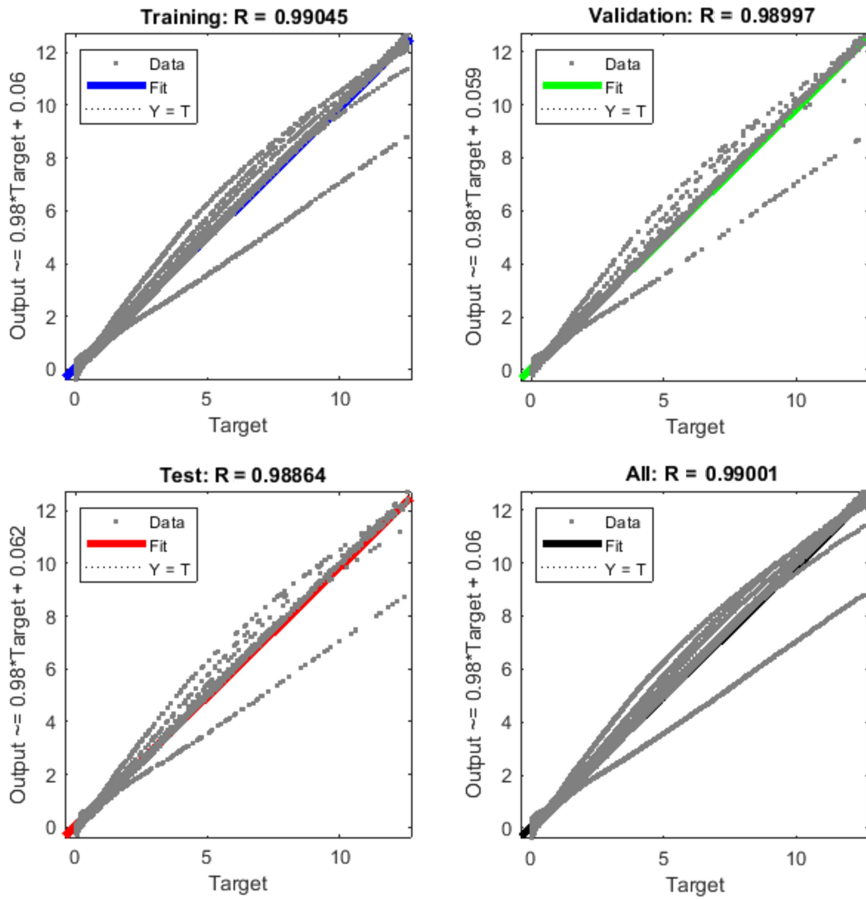


FIG. 5. Linear regression of outputs versus targets for the ANN with 15 neurons in the hidden layer: top left for the training stage, top right for the validation stage, bottom left for the test stage and bottom right for all data.

network’s structure should be adjusted in terms of the number of neurons in the hidden layer.

Further analysis of Fig. 5 leads to the observation that ( $\sim 4 - \sim 9$ ) MPa is the stress region, which is the least fitted. This interval can be identified as the second part of the plateau region and the beginning of the post-plateau region in the stress-strain plot (compare: Fig. 2). This indicates that data might require trunking into sets with regard to characteristic stress intervals.

Moreover, in Fig. 5, it is visible that one sample was problematic for the network to fit. One cannot uniquely identify which of the samples caused this; however, it could be one of the two specimens which had an apparent density of  $0.36 \text{ g/cm}^3$ . This assumption is based on the fact that in spite of equal apparent densities, the compressive responses of the discussed samples were not identical

(see Fig. 2). This might be attributed to the fact that one of the specimens belonged to the prototype group and the other to the regular group. Thus, introducing a third entry in  $\mathbf{Input}_i$  vectors, along with strain and apparent density, which would indicate whether a sample belonged to the 'P' or 'R' group, could improve ANN analysis results.

**Errors.** Errors are defined as the difference between a target and the corresponding network's output:

$$(3.3) \quad \text{Err}_i = \sigma_i - \sigma_{i,\text{otpt}}.$$

Error histograms for both networks are depicted in Fig. 6. It can be seen that the proportion of error instances between the three steps, namely: training (blue),

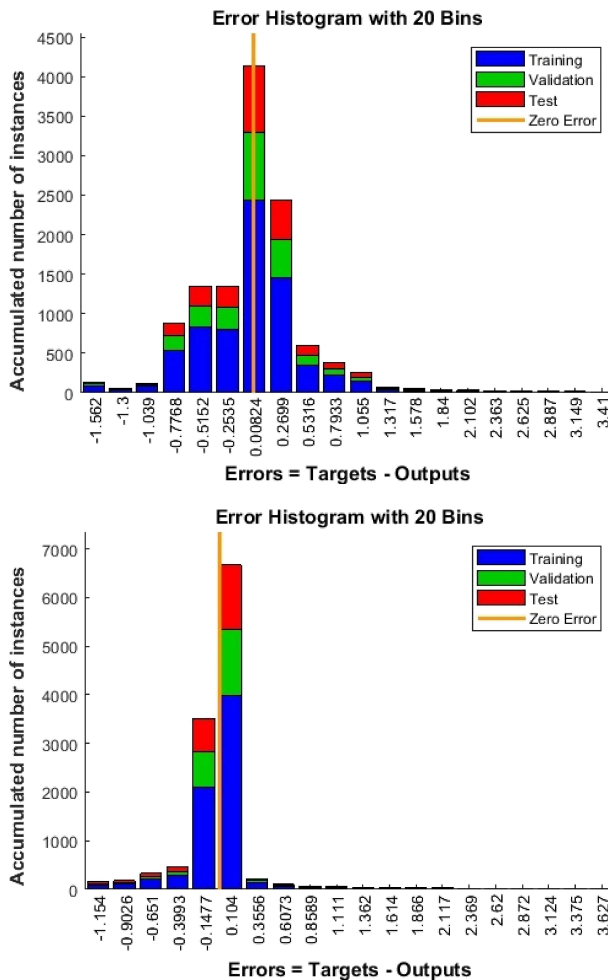


FIG. 6. Error histograms: top for the ANN with 3 neurons in the hidden layer; bottom for the ANN with 15 neurons in the hidden layer.

validation (green) and test (red), is very much about equal to the proportion between input data for each of them (60% : 20% : 20% respectively). This fact implies that the assumed training algorithm is appropriate, since it results in a uniform propagation of errors onto the data sets.

In both used networks the distribution of errors has a clear maximum of instances which is located around the zero error ( $Err = 0$ ). This can be interpreted as a good potential of the used algorithm for the convergence between outputs and targets.

As for the ranges with most error instances, in the case of the 3 neurons network errors occur in a broader interval than in the 15 neurons network:

$$Err_{3n}^{most} \in [-0.7768; 0.5316],$$

$$Err_{15n}^{most} \in [-0.1477; 0.104],$$

which confirms the earlier conclusion (in the previous Paragraph: *The relation...*) on the need of adjustment of the ANN structure in terms of the number of neurons.

**Relative errors.** Absolute relative errors are defined as the absolute value of the ratio of the difference between a target and the corresponding network's output over the target:

$$(3.4) \quad ARE_i = \left| \frac{\sigma_i - \sigma_{i,opt}}{\sigma_i} \right|.$$

Figure 7 depicts histograms of absolute relative errors for networks with 3 (top) and 15 (bottom) neurons. Data for all learning stages – training, validation and test – are depicted together with one colour. The graphs are truncated at  $ARE = 3$  (in order to give better clarity of the graphical representation); however, only 12 instances of  $ARE_i$  were larger than 3 for each network. A large majority of  $ARE_i$  was smaller than 7.5%: the number of such instances for the network with 3 neurons was more than 9000, on the other hand, the respective number of instances for the network with 15 neurons was about 9800.

Additionally, mean absolute relative error was calculated according to the following formula:

$$(3.5) \quad MARE = \frac{\sum_{i=1}^n ARE_i}{n},$$

where  $i = 1, 2, \dots, n$ , with  $n = 12000$ .

The obtained values of MARE were:  $MARE_{3n} = 27.545\%$  and  $MARE_{15n} = 9.251\%$ . The result for the ANN with 3 neurons is not satisfactory.  $MARE_{15n}$

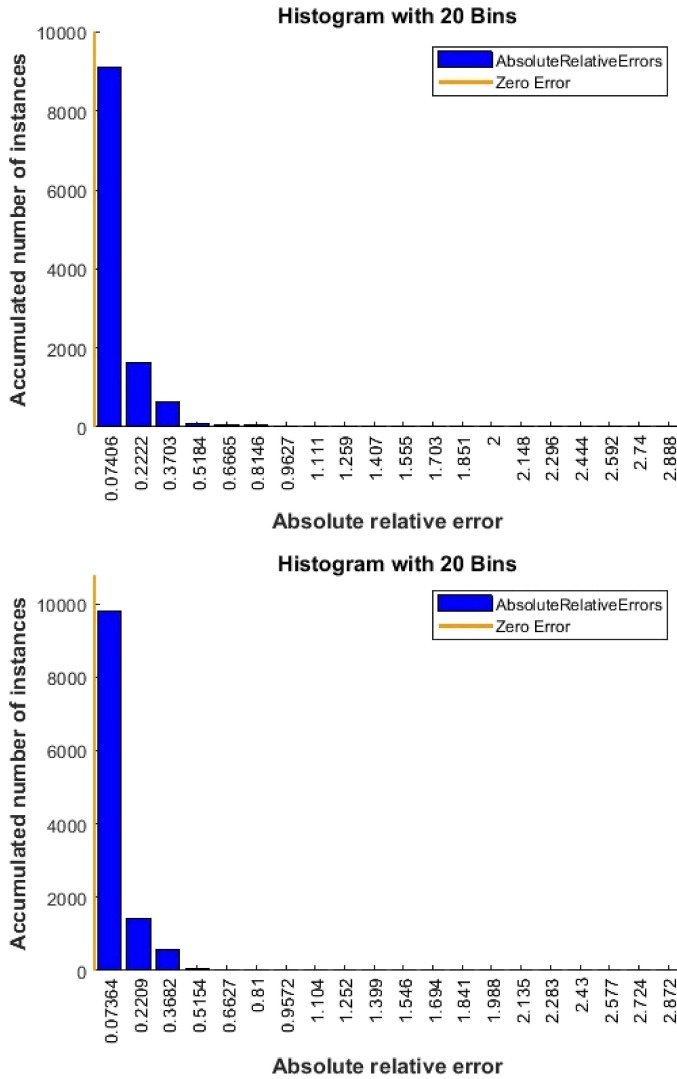


FIG. 7. Absolute relative error histograms: top for the ANN with 3 neurons in the hidden layer; bottom for the ANN with 15 neurons in the hidden layer.

would be acceptable in case of rough engineering applications (less than 10%), but for more reliable modelling, the network structure should be adjusted. However, obtaining a single-digit result in the preliminary study is promising and confirms that with a better calibration of network parameters the approximation could reach a very good level.

**Network’s performance and MSE.** A standard choice of the performance index in multilayer networks is MSE [37]. Hence, this magnitude was assumed

as the performance function in the present study. The mathematical expression for MSE was:

$$(3.6) \quad \text{MSE} = \frac{\sum_{i=1}^n (\sigma_i - \sigma_{i,\text{opt}})^2}{n},$$

where  $i = 1, 2, \dots, n$ , with  $n = 12000$ .

The goal for the performance function was set as 0 and the number of validation failures was set as 6. Figure 8 presents the course of the performance function

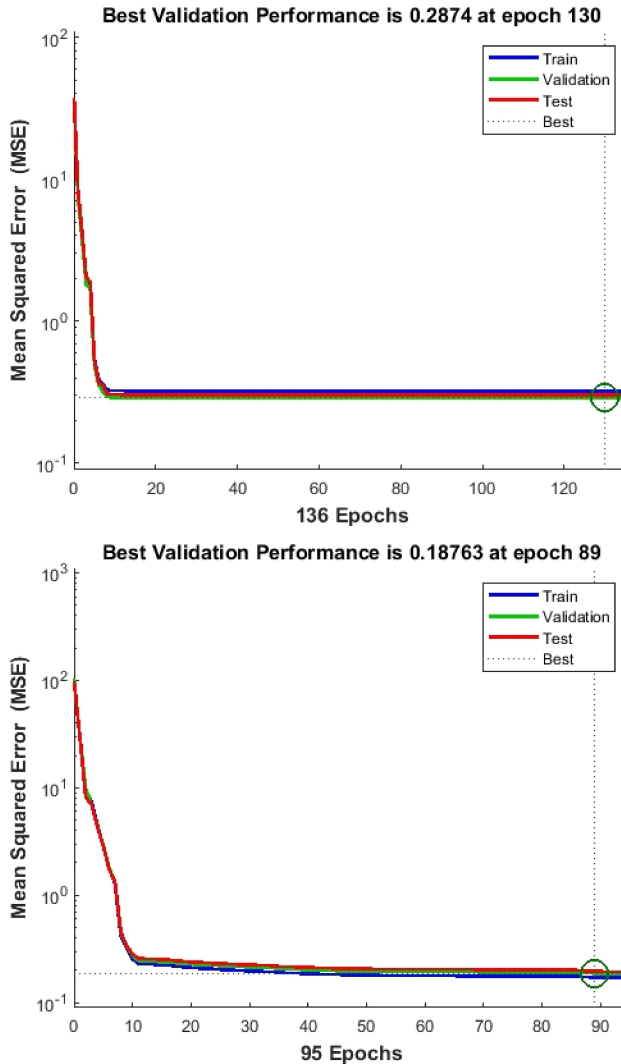


FIG. 8. The course of the performance function: top for the ANN with 3 neurons in the hidden layer; bottom for the ANN with 15 neurons in the hidden layer.

with regard to epochs. Circles mark the achievement of the validation failures number during the pursuit of the goal. In the case of the 3 neurons network the best obtained MSE in the validation stage was  $\text{MSE}_{3n}^{\text{valid.best}} = 0.2874 \text{ MPa}^2$  and it was achieved for the epoch number 130. For the ANN with 15 neurons the result was  $\text{MSE}_{15n}^{\text{valid.best}} = 0.18763 \text{ MPa}^2$ , for the epoch no. 89.

MSE was also assumed as one of the auxiliary criteria for the assessment of the quality of the approximation. However, this time MSE was calculated for all learning stages together. The obtained results were  $\text{MSE}_{3n} = 0.3107 \text{ MPa}^2$  and  $\text{MSE}_{15n} = 0.1796 \text{ MPa}^2$ . One can observe that the more complex network produced better results, which indicates that the approximated function is rather more complex than simple and confirms that adjustment of the number of neurons in the hidden layer could be required.

#### 4. CONCLUSIONS

Comparison between results for the two investigated networks – with 3 and 15 neurons in the hidden layers – show that more neurons produced better approximation:  $R_{3n}^2 = 0.96560$  and  $R_{15n}^2 = 0.98011$ ;  $\text{MARE}_{3n} = 27.545\%$  and  $\text{MARE}_{15n} = 9.251\%$ ;  $\text{MSE}_{3n} = 0.3107 \text{ MPa}^2$  and  $\text{MSE}_{15n} = 0.1796 \text{ MPa}^2$ . This indicates that one of the objectives in further research should be the adjustment of the number of neurons. It seems that calibration of other network architecture or learning parameters, like, e.g., validation threshold or proportion of data designated for each learning stage, could lead to a better quality of modelling [45].

As for the data, the following aspects also need to be included in future research. First, the data chosen for the present study was from compressive experiments for samples which had some imperfections, which might have influenced the modelling. This fact could be included in the introduction of the third input variable, which would indicate to which of the groups a considered sample belonged. Also, the compressive behaviour has clear phases (initial slope of the stress-strain curve, plateau and ‘hardening’) and those phases were also reflected in the ANN target-output accuracy analysis; hence, data grouping into intervals should be taken under consideration.

In the end, a general conclusion can be posed that the obtained results ( $R_{15n}^2 > 96\%$  and  $\text{MARE}_{15n} < 10\%$ ) confirm that Relation 3.1:  $\sigma = f(\epsilon, \rho)$  can model the compression of open-cell aluminium with the use of ANN. Verification of this hypothesis was the aim of the presented research. Networks used in the study were two-layer feedforward networks with tansig activation function in the hidden layers and linear activation function in the output layers.

## ACKNOWLEDGEMENTS

The authors would like to acknowledge that the production of aluminium samples and experimental tests were partially supported by the Faculty of Mechanical Engineering and Robotics of the AGH University of Science and Technology (grant no. 15.11.130.488). The authors would like to express their gratitude to Recticel Flexible Foams, Belgium, for providing precursors for the production of aluminium samples.

## REFERENCES

1. DEGISCHER H., KRISZT B., *Handbook of cellular metals: production, processing, applications*, Wiley-VCH Verlag GmbH & Co. KGaA, Weinheim, 2002.
2. GARCÍA-MORENO F., *Commercial applications of metal foams: their properties and production*, *Materials*, **9**(2): 85–111, 2016.
3. SOB CZAK J., WOJCIECHOWSKI A., BOYKO L., DRENCHEV L., DARŁAK P., DUDEK P., *Highly porous materials* [in Polish: *Materiały wysokoporowate*], Instytut Odlewnictwa, Kraków, 2005.
4. SIMANCIK F., JERZ J., KOVÁČIK J., MINÁR P., *Aluminium foam – a new light-weight structural material*, *Kovové Materiály (Metallic Materials)*, **35**: 265–277, 1997.
5. *Duocel® copper foam*, ERG Materials and Aerospace Corp., Oakland, CA 94608, US, <https://ergaerospace.com/materials/duocel-copper-foam> (accessed 15 Oct. 2018).
6. DUNAND D.C., *Processing of titanium foams*, *Advanced Engineering Materials*, **6**(6): 369–376, 2004.
7. JAKUBOWICZ J., ADAMEK G., DEWIDAR M., *Titanium foam made with saccharose as a space holder*, *Journal of Porous Materials*, **20**(5): 1137–1141, 2013.
8. BANHART J., *Gold and gold alloy foams*, *Gold Bulletin*, **41**(3): 251–256, 2008.
9. SMITH B.H., SZYNISZEWSKI S., HAJJAR J.F., SCHAFER B.W., ARWADE S.R., *Steel foam for structures: A review of applications, manufacturing and material properties*, *Journal of Constructional Steel Research*, **71**: 1–10, 2012.
10. DUARTE I., OLIVEIRA M., *Aluminium alloy foams: production and properties*, [in:] K. Kon-doh [Ed.], *Powder Metallurgy*, InTech, pp. 47–72, 2012.
11. NIEH T.G., HIGASHI K., WADSWORTH J., *Effect of cell morphology on the compressive properties of open-cell aluminum foams*, *Materials Science and Engineering: A*, **283**(1–2): 105–110, 2000.
12. MIEDZIŃSKA D., NIEZGODA T., GIELETA R., *Numerical and experimental aluminum foam microstructure testing with the use of computed tomography*, *Computational Materials Science*, **64**: 90–95, 2012.
13. ZHOU J., SHROTRIYA P., SOBOYEJO W.O., *Mechanisms and mechanics of compressive deformation in open-cell Al foams*, *Mechanics of Materials*, **36**(8): 781–797, 2004.

14. PAPADOPOULOS D.P., OMAR H., STERGIODI F., TSIPAS S.A., LEFAKIS H., MICHALIDIS N., *A novel method for producing Al-foams and evaluation of their compression behavior*, Journal of Porous Materials, **17**(6): 773–777, 2010.
15. WICKLEIN M., THOMA K., *Numerical investigations of the elastic and plastic behaviour of an open-cell aluminium foam*, Materials Science and Engineering: A, **397**(1–2): 391–399, 2005.
16. ROBERTSON I.M. *et al.*, *Towards an integrated materials characterization toolbox*, Journal of Material Research, **26**(1): 1341–1383, 2011.
17. KURZYŃSKI M., *Methods of artificial intelligence for engineers* [in Polish: *Metody sztucznej inteligencji dla inżynierów*], Państwowa Wyższa Szkoła Zawodowa im. Witelona w Legnicy, Stowarzyszenie „Wspólnota Akademicka”, Legnica, 2008.
18. LEFIK M., *Application of artificial neural networks in mechanics and engineering* [in Polish: *Zastosowanie sztucznych sieci neuronowych w mechanice i w inżynierii*], Wydawnictwo Politechniki Łódzkiej, Łódź, 2005.
19. JAKUBEK M., *Application of artificial neural networks in selected problems of experimental mechanics and structural engineering* [in Polish: *Zastosowanie sztucznych sieci neuronowych w wybranych zagadnieniach eksperymentalnej mechaniki materiałów i konstrukcji*], PhD thesis, Politechnika Krakowska, Kraków, 2007.
20. PIETRZYK M., KUSIAK J., SZELIGA D., RAUCH Ł., SZTANGRET Ł., GÓRECKI G., *Application of metamodels to identification of metallic materials models*, Advances in Materials Science and Engineering, **2016**, article ID: 2357534, 20 pages, 2016.
21. STREK A.M., *Assessment of strength and functional properties of cellular materials* [in Polish: *Ocena właściwości wytrzymałościowych i funkcjonalnych materiałów komórkowych*], PhD thesis, AGH, Kraków, 2017.
22. KASZA P., LIPOWSKA B., PECHERSKI R.B., STREK A.M., WAŃCZYK K., *Compression of open-cell aluminium*, Engineering Transactions, **64**(4): 629–634, 2016.
23. STREK A.M., LIPOWSKA B., WAŃCZYK K., *Selected aspects of manufacturing of aluminium sponge*, Archives of Metallurgy and Materials, **64**(3), 2019 (accepted, in print).
24. BANHART J., *Manufacture, characterisation and application of cellular metals and metal foams*, Progress in Materials Science, **46**(6): 559–632, 2001.
25. KRÄNZLIN N., NIEDERBERGER M., *Controlled fabrication of porous metals from the nanometer to the macroscopic scale*, Materials Horizons, **2**: 359–377, 2015.
26. KANAUN S., TKACHENKO O., *Representative volume element and effective elastic properties of open cell foam materials with random microstructures*, Journal of Mechanics of Materials and Structures, **2**(8): 1607–1628, 2007.
27. ISO 13314:2011, *Mechanical testing of metals – Ductility testing – Compression test for porous and cellular metals*, International Organization for Testing, 2011.
28. JANG W.-Y., KRAYNIK A.M., KYRIAKIDES S., *On the microstructure of open-cell foams and its effect on elastic properties*, International Journal of Solids and Structures, **45**(7–8): 1845–1875, 2008.

29. GIBSON I.J., ASHBY M.F., *The mechanics of three-dimensional cellular materials*, Proceedings of the Royal Society A, **382**(1782): 43–59, 1982.
30. DUDZIK M., MIELNIK R., WRÓBEL Z., *Preliminary analysis of the effectiveness of the use of artificial neural networks for modelling time-voltage and time-current signals of the combination wave generator*, [in:] SPEEDAM 2018 – Proceedings: International Symposium on Power Electronics, Electrical Drives, Automation and Motion, 8445277, pp. 1095–1100, 2018.
31. DUDZIK M., TOMCZYK K., JAGIELLO A.S., *Analysis of the error generated by the voltage output accelerometer using the optimal structure of an artificial neural network*, [in:] Proceedings of the 19th International Conference on Research and Education in Mechatronics, REM 2018, 8421789, pp. 7–11, 2018.
32. DUDZIK M., MIELNIK R., WRÓBEL Z., *Preliminary analysis of the effectiveness of the use of artificial neural networks for modeling time-voltage signal of the combination wave generator*, 18th International Symposium on Electromagnetic Fields in Mechatronics, Electrical and Electronic Engineering, ISEF 2017, 8090698, 2017.
33. McCAFFREY J., *How to standardize data for neural networks*, Visual Studio Magazine 01/15/2014, <https://visualstudiomagazine.com/articles/2014/01/01/how-to-standardize-data-for-neural-networks.aspx> (accessed 15 Sept 2018).
34. DEMUTH H., BEALE M., HAGAN M., *Neural Network Toolbox 5 User's Guide*, The MathWorks Inc., 2007.
35. Mathworks documentation: mapminmax, <https://www.mathworks.com/help/deeplearning/ref/mapminmax.html> (accessed 21 Feb 2019).
36. *Matlab and automatic target normalization: mapminmax. Don't trust your Matlab framework!*, <https://neuralsniffer.wordpress.com/2010/10/17/matlab-and-automatic-target-normalization-mapminmax-donttrust-your-matlab-framework/> (accessed 21st Feb 2019).
37. HAGAN M.T., DEMUTH H.B., BEALE M.H., DE JESUS O., *Neural network design*, 2nd Ed., eBook, 2014.
38. LEVENBERG K., *A method for the solution of certain non-linear problems in least squares*, Quarterly of Applied Mathematics, **2**: 164–168, 1944.
39. MARQUARDT D.W., *An algorithm for least-squares estimation of nonlinear parameters*, SIAM Journal on Applied Mathematics, **11**(2): 431–441, 1963.
40. MADSEN K., NIELSEN H.B., TINGLEFF O., *Methods for non-linear least squares problems*, Informatics and Mathematical Modelling Technical University of Denmark, 2nd Ed., April 2004, [http://www2.imm.dtu.dk/pubdb/views/edoc\\_download.php/3215/pdf/imm3215.pdf](http://www2.imm.dtu.dk/pubdb/views/edoc_download.php/3215/pdf/imm3215.pdf) (accessed 15 Oct 2018).
41. *Levenberg-Marquardt algorithm*, article in Wikipedia, on-line: [https://en.wikipedia.org/wiki/Levenberg-Marquardt\\_algorithm](https://en.wikipedia.org/wiki/Levenberg-Marquardt_algorithm) (accessed 15 Oct 2018).
42. GIRARD A., *Excerpt from theoretical and instrumental optics review* [in French: *Excerpt from Revue d'optique théorique et instrumentale*], *Revue d'Optique*, **37**: 225–241, 397–424, 1958.

43. WYNNE C.G., *Lens designing by electronic digital computer: I*, Proceedings of the Physical Society of London, **73**(5): 777–787, 1959.
44. MORRISON D.D., *Methods for nonlinear least squares problems and convergence proofs*, [in:] Proceedings of the Jet Propulsion Laboratory Seminar on Tracking Programs and Orbit Determination, Pasadena, California, pp. 1–9, 1960.
45. DUDZIK M., STREK A.M., *ANN architecture specifications for modelling of open-cell aluminium under compression*, 2019 (in preparation).

*Received December 4, 2018; accepted version May 12, 2019.*

---

*Published on Creative Common licence CC BY-SA 4.0*

